DOI 10.5012/bkcs.2011.32.8.2671

Charge Transport Characteristics of Dye-Sensitized TiO_2 Nanorods with Different Aspect Ratios

Eun Yi Kim,[†,‡] Wan In Lee,[†] and Chin Myung Whang[‡,*]

[†]Department of Chemistry, [‡]School of Materials Science and Engineering
Inha University, Incheon 402-751, Korea. [*]E-mail: cmwhang@inha.ac.kr
Received May 29, 2011, Accepted June 27, 2011

Nanocrystalline TiO_2 spherical particle (NP) with a dimension of 5 × 5.5 nm and several nanorods (NR) with different aspect ratios (diameter × length: 5 × 8.5, 4 × 15, 4 × 18 and 3.5 × 22 nm) were selectively synthesized by a solvothermal process combined with non-hydrolytic sol-gel reaction. With varying the molar ratio of TTIP to oleic acid from 1:1 to 1:16, the NRs in the pure anatase phase were elongated to the c-axis direction. The prepared NP and NRs were applied for the formation of nanoporous TiO_2 layers in dye-sensitized solar cell (DSSC). Among them, NR2 (TiO_2 nanorod with 4 × 15 nm) exhibited the highest cell performance: Its photovoltaic conversion efficiency (η) of 6.07%, with J_{sc} of 13.473 mA/cm^2, V_{oc} of 0.640 V, and FF of 70.32%, was 1.44 times that of NP with a size of 5 × 5.5 nm. It was observed from the transient photoelectron spectroscopy and the incident photon to current conversion efficiency (IPCE) spectra that the TiO_2 films derived from NR2 demonstrate the longest electron diffusion length (L_e) and the highest external quantum efficiency (EQE).

Key Words : Dye-sensitized solar cell, TiO_2 nanorods, Charge transport

Introduction

Since the first report in 1991 by O'Regan and Grätzel,[1] dye-sensitized solar cell (DSSC) has attracted a lot of interest over the last decade due to its relatively high conversion efficiency, low cost, and simple preparation procedure. In general, DSSC consists of nanoporous TiO_2 electrode, light-absorbing dye, electrolytes, and counter electrode (CE), and TiO_2 electrode is regarded to be one of the key components. The roles of TiO_2 are adsorption of dye molecules, transport of electrons from dye to transparent conductive oxide (TCO), and allowance of electrolyte diffusion from CE to dye molecules. The amount of dye adsorbed on the surface of TiO_2 will determine the absorption efficiency of sunlight, which is related to the number of electrons generated in the cells. Most of all, the structure and shape of TiO_2, used for the formation of the dye-absorbing electrode, will critically affect the pore size distribution, porosity, and connectivity among TiO_2 nanocrystals, all of which will be correlated to the transport of electrons and the diffusion of electrolytes in the cells.[2]

Thus far there were various reports on the improvement of TiO_2 photoelectrode system by tailoring of particle size and morphology,[3,4] modification of electrode structure and fabrication procedure,[5] suppress of charge recombination,[6,7] interfacial control,[8] and others. In general, TiO_2 electrodes have been prepared from the spherical nanoparticles by doctor-blade technique, which is a convenient method to form nanoporous electrodes with high surface areas. Recently, several one dimensional (1D) TiO_2 nanomaterials, such as nanowires,[9] nanotubes[10] and nanorods[11-13] have been synthesized and applied to the DSSCs, because they can offer direct-electron-pathways to the TCO. Most of them are TiO_2 nanorod[14] and nanotube[15] arrays prepared by anodic oxidation method, TiO_2 nanorods or nanowires synthesized from wet-chemistry,[16,17] and composite of TiO_2 nanoparticles and nanorods.[18,19] In most case, however, photovoltaic conversion efficiencies of DSSCs with these 1D TiO_2 nanocrystals are not as high as that of the cell with nanoparticles. Presumably this is due to the decrease in the specific surface area to accommodate dye molecules and the relatively poor contact at the interface or among the 1D TiO_2 nanocrystals, although their 1D structures with less grain boundary and less defect sites are highly advantageous to the electron transport. In order to achieve high efficiency DSSC, we believe that above mentioned conflicting properties of TiO_2 nanocrystals have to be optimized by controlling the nanorod length or aspect ratio.

In the present work, nanocrystalline TiO_2 spherical particle (NP) and nanorods (NR) with tunable aspect ratios were successfully synthesized by a solvothermal reaction, and they were applied as photoelectrodes of DSSCs. The photovoltaic properties depending on the length of NR were analyzed, and their electron-transporting behaviors were examined by several spectroscopic techniques.

Experimental

Preparation of TiO_2 Photoelectrode on the FTO Glass Substrate. The nanocrystalline TiO_2 with tunable aspect ratios were synthesized by a solvothermal reaction. Titanium isopropoxide ($Ti[OCH(CH_3)_2]_4$, 97%, Aldrich, TTIP) and oleic acid ($CH_3(CH_2)_7CH=CH(CH_2)_7COOH$, 90%, Aldrich) and butyl ether ($C_4H_9OC_4H_9$, 99%, Aldrich) were used as

the precursor, surfactant and solvent, respectively. The detailed synthetic procedure is described in a previous work.[20] The mixtures of TTIP and oleic acid with the molar ratio from 1:1 to 1:16 were stirred for 1 h, and then transferred to an autoclave. For the solvothermal reaction, the temperature of the autoclave was raised to 250, 280 or 300 °C at a rate of 5 °C/min, and held for 4, 6, 12, 24 or 48 h. After solvothermal reaction, the prepared TiO_2 NP or NRs were collected by centrifugation, and washed with ethanol several times.

Fabrication of DSSC. For the preparation of TiO_2 NP or NRs, a viscous paste was prepared by the following procedure. A mixture of 0.3 g ethyl cellulose and 4.5 g terpineol was added to 10 mL ethanol suspension containing 1.5 g TiO_2 NP or NRs, and then mixed in a paste mixer (PDM-300, Dae-wha Tech.) at 1100 rpm for 90 min. The prepared TiO_2 paste was coated on the pre-cleaned FTO film using the doctor blade method. The coated films were baked at 110 °C for 30 min and subsequently calcined at 500 °C for 15 min. For dye adsorption, the fabricated TiO_2 films were immersed in anhydrous ethanol solution 0.3 mM N719 dye (Solaronix Co.) for over 24 h at room temperature. Pt-coated FTO, used as CE, was prepared by dropping a 0.7 mM H_2PtCl_6 solution on an FTO glass. These samples were heated at 400 °C for 30 min in air. An iodide-based solution was used as the liquid electrolyte, 0.6 M tetra-butyl-ammonium iodide ($[CH_3(CH_2)_3]_4NI$, Sigma-Aldrich, 98%), 0.1 M lithium iodide (LiI, Sigma-Aldrich, 99.9%), 0.1 M iodine (I_2, Sigma-Aldrich, 99.8%), and 0.5 M 4-*tert*-butyl pyridine ($C_9H_{13}N$, Sigma-Aldrich, 99%) in acetonitrile (CH_3CN, Aldrich, 99%).

Characterization. X-ray Diffraction (Regaku, DMAX2500) was used to verify the phase, crystal structure, and particle size of the TiO_2 nanocrystal powders and films. The size and shape of the TiO_2 nanoparticles and nanorods were analyzed by transmission electron microscopy (TEM, Philips CM30). The thickness of TiO_2 films were investigated by scanning electron microscopy (SEM, Jeol 5500).

Photocurrent-voltage (I-V) measurements were performed using a Keithley model 2400 source measurement unit. A 300 W Xenon lamp (Spectra-Physics) was used as a light source and its light intensity was adjusted using an NREL-calibrated Si solar cell equipped with a KG-5 filter for approximating AM 1.5G one sun light intensity. Electrical impedance spectra were measured with an impedance analyzer (Compactstat, IVIUM Tech.) at open-circuit potential under AM 1.5G one sun light illumination, with frequency ranging from 10^{-1} Hz to 10^6 Hz. The magnitude of the alternative signal was 10 mV. Impedance parameters were determined by fitting of impedance spectra using Z-view software. The incident photon to current efficiency (IPCE) spectra was measured as a function of wavelength from 400 nm to 900 nm using a specially designed IPCE system for dye-sensitized solar cell (PV Measurements, Inc.). The electron diffusion coefficient and the electron lifetime were measured by a laboratory-made stepped light-induced transient measurements of photocurrent (SLITMP) technique, proposed by Yanagida *et al*..[21] The diode laser (Coherent, LaLaser, λ = 635 nm) was employed for both the photocurrent and voltage transient. Typically, the laser was operated at the voltage of 3.10 V and stepped down to 3.00 V, which provides a laser power of approximately 6.6 mW. The transients were induced by the stepwise change of the laser intensity with a set of ND filters.

Results and Discussion

Morphology and Crystal Structure of the TiO_2 Nanorods. TiO_2 nanoparticles and several nanorods in the pure anatase phase were reproducibly synthesized by a solvothermal process with controlling the concentration of carboxylic acids, the kind of carboxylic acids, and reaction temperatures. During solvothermal process, esterification reactions between the carboxyl groups of oleic acid and the alkyl groups of TTIP were considered to be a key factor in controlling the size and shape of TiO_2 nanocrystals. The growth mechanisms of TiO_2 nanorods were described in detail in the previous report.[20]

Figure 1 shows the TEM images of the TiO_2 nanocrystals in spherical and rod shapes. By varying the reaction parameters during solvothermal reaction, the lengths of the nanocrystals were controlled in the range of 5.5-22 nm, whereas their diameters were remained in 3.5-5 nm. It was found that the concentration of the oleic acids strongly

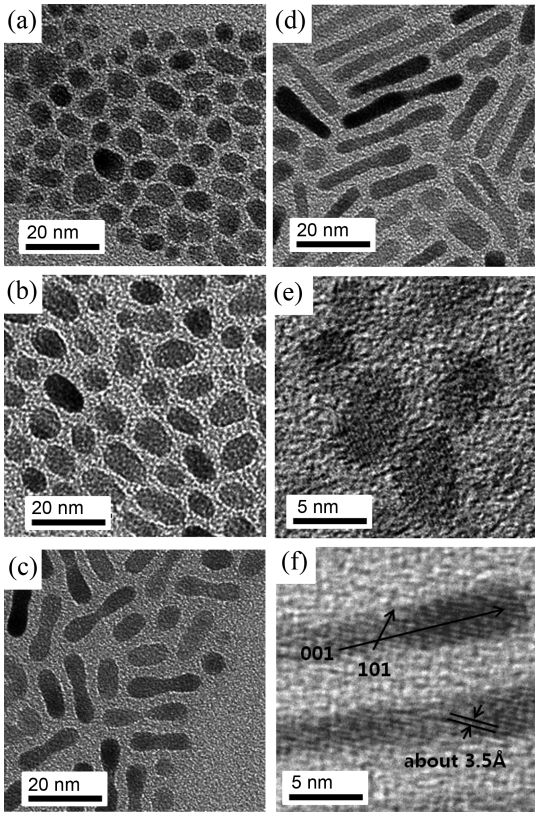

Figure 1. TEM images of the as-prepared TiO_2 nanocrystals with different lengths and diameters. (a) 5 × 5.5 nm (NP); (b) 5 × 8.5 nm (NR1); (c) 4 × 15 nm (NR2); (d) 3.5 × 22 nm (NR4). (e) and (f) are high resolution TEM images of (a) and (d), respectively.

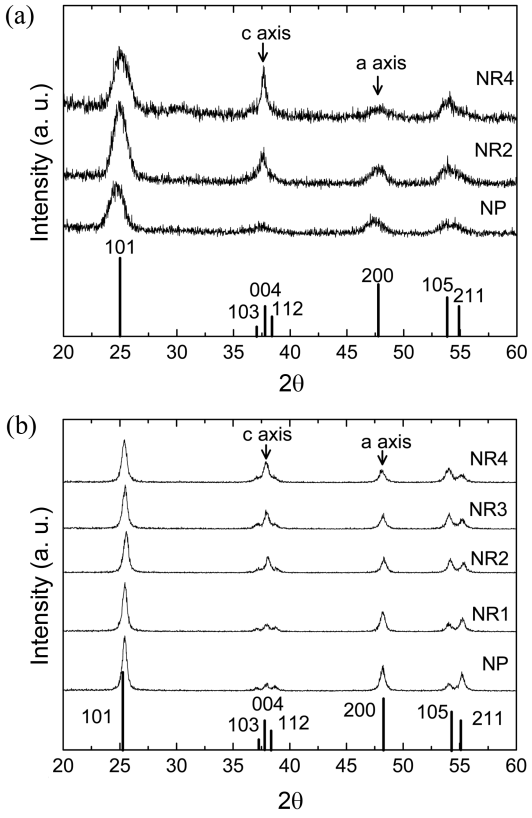

Figure 2. XRD patterns of (a) the as-prepared TiO_2 nanocrystals with different lengths and (b) the TiO_2 nanocrystal-based 16 mm-thick films heat-treated at 500 °C.

influenced the aspect ratio of the synthesized TiO_2 nanorods. With changing the molar ratio of TTIP:oleic acid from 1:1 to 1:4, 1:8 and 1:16, the 5 × 5.5 nm-sized spherical TiO_2 was elongated to 4 × 8.5 nm, 4 × 15 nm, and 3.5 × 22 nm-sized nanorods, respectively.

As shown in Figure 2(a), X-ray diffraction patterns of the TiO_2 nanocrystals indicate that the prepared nanocrystals are in the pure anantase phase and are grown anisotropically along the c-axis. NR4, the longest NR with 3.5 × 22 nm, exhibits the highest ratio of (004)/(200) peaks among the nanocrystals. The gradual increase in the relative intensity ratios of (004)/(200) peaks indicates that the initially formed spherical TiO_2 was extended to nanorod structures as a consequence of the grain growth along the [001] direction.[2]

For the application to the DSSC photoelectrode, TiO_2 pastes, prepared from the several TiO_2 nanocrystals, were coated on the FTO glass and subsequently calcined at 500 °C for 30 min. To estimate the structural change by heat-treatment, the TiO_2 films with ~16 mm-thickness were analyzed by XRD. As shown in Figure 2(b), the crystallinities of TiO_2 were considerably increased, suggesting that the individual particles are sintered and merged to form larger anatase grains. Although the intensity ratios of (004)/(200) were decreased, the anisotropic character of NRs, grown to the [001] direction, was still maintained in the fabricated TiO_2 films. The detailed characterization results are described in Table 1.

Application to DSSC Photoelectrodes. Figure 3 shows the photocurrent (I) – photovoltage (V) characteristics for the cells derived from the several NRs and NP with approximately 16 μm in film thickness. The TiO_2 nanorod-based DSSC (DSSC-NR) exhibited relatively higher J_{sc} than those from the nanoparticle (DSSC-NP), and J_{sc} was also dependent on the NR length. NR2 sample (length × diameter: 4 × 15 nm) showed the highest J_{sc} with 13.473 mA/cm^2, whereas the longer NRs provided relatively lower J_{sc}, as indicated in Figure 3. Contrarily, V_{oc} of the DSSC-NR was slightly lower than that of DSSC-NR in all cases, and it was gradually decreased as the NR length increased. This suggests that more resistance is applied to the FTO/TiO_2 interface, considering that long NR will be difficult to completely cover the entire FTO glass. That is, some area of FTO would not be covered with TiO_2, and as a result, the electrons transported to FTO from the TiO_2 CB could be back-transported to the electrolyte such as I_3^-.

Figure 4 shows the Nyquist plots for several DSSCs analyzed by the electrical impedance spectroscopy (EIS). In

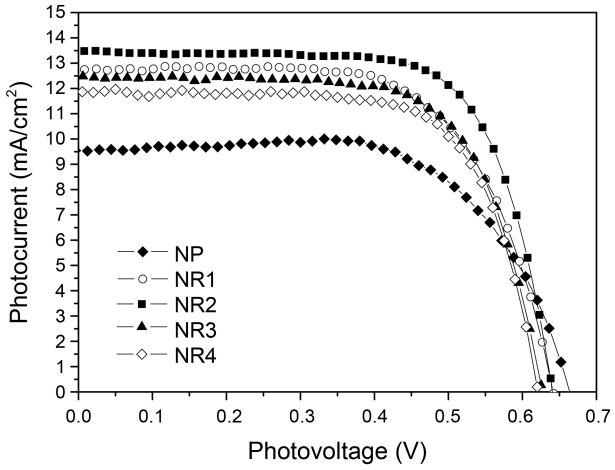

Figure 3. I-V characteristics for the DSSCs fabricated from several TiO_2 nanocrystals measured under 1 sun illumination. The thicknesses of the NP and NRs were approximately 16 μm.

Table 1. Intensity ratios of (004)/(200) XRD peaks for the TiO_2 nanocrsytals

Sample name		NP	NR1	NR2	NR3	NR4
Diameter (nm × nm)		5 × 5.5	5 × 8.5	4 × 15	4 × 18	3.5 × 22
Intensity ratio of (004)/(200) peaks	I_{solv}[a]	0.54	0.98	1.95	3.08	4.56
	I_{heat}[b]	0.32	0.35	1.14	1.16	1.56

[a]Intensity ratio of the TiO_2 nanocrystals after solvothermal process without any treatment. [b]Intensity ratio of the TiO_2 nanocrystal-based films after heat-treatment at 500 °C

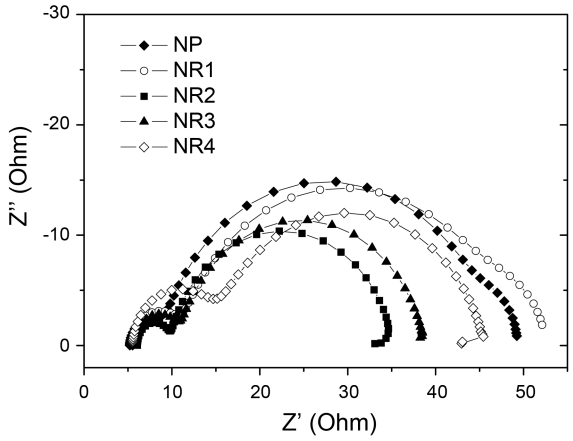

Figure 4. Electron impedance spectra of the DSSCs derived from several TiO_2 nanocrystals.

Table 2. Photovoltaic performance and interface resistance of the DSSCs derived from several TiO_2 nanocrystals

Sample	V_{oc} (V)	J_{sc} (mA/cm^2)	FF (%)	η (%)	R_1 (Ω)[a]	R_2 (Ω)[b]
NP	0.6643	9.536	66.01	4.18	3.53	37.53
NR1	0.6417	12.751	65.12	5.33	3.62	36.21
NR2	0.6404	13.473	70.32	6.07	4.83	25.57
NR3	0.6266	12.485	68.16	5.33	5.34	28.03
NR4	0.6212	11.833	69.88	5.14	9.18	27.88

[a]Resistance applied to the FTO/TiO_2 interface. [b]Resistance applied to the TiO_2/electrolyte interface

general, three semicircles are observed from a Nyquist plot. The semicircle in the high frequency region (10^4-10^2 Hz) represents the resistance applied to the Pt CE, TiO_2 electrode, and/or the interface between FTO and TiO_2 layers,[22-24] whereas those in the intermediate frequency (-10^1 Hz) and the low frequency (-10^0 Hz) region offer information on the resistances at the TiO_2/electrolyte interface and the Nernst diffusion of the electrolyte, respectively.[21,25,26] It was found that the semicircles in the high frequency region were increased, as the lengths of the NRs increased. As a result, NR4-based DSSC exhibited the largest semicircle with resistance of 9.18 Ω, suggesting that the resistance applied to the FTO/TiO_2 interface was considerably increased due to the difficulty in packing long NRs on the FTO glass. On the other hand, the resistance at the TiO_2/electrolyte interface for the NR4 sample was relatively smaller than that of the NP or shorter NR samples, as indicated in Table 2. This suggests that the photo-injected electrons on NR4 layer are prone to be lost by the back-reaction to electrolyte, which would be caused by the long retention time of electrons in TiO_2 layer due to the high resistance in the interface with FTO.

The electron diffusion in the TiO_2 layer during the DSSC operation was analyzed by the SLITMP technique.[21] The electron diffusion coefficient (D_e) was determined by the following equation;

$$D_e = L^2/(2.77\tau_c) \quad (1)$$

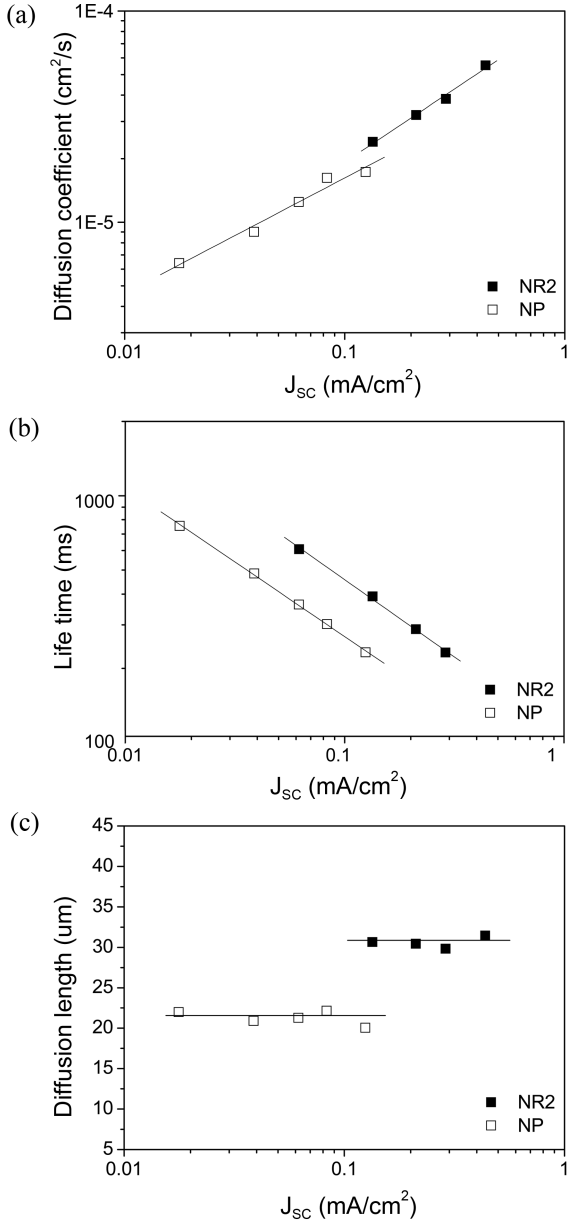

Figure 5. (a) Electron diffusion coefficient (D_e), (b) electron life time (t_e) and (c) electron diffusion length (L_e) for the DSSC-NP and DSSC-NR2 as a function of J_{sc}.

where L and τ_c are the film thickness and time constant, respectively. τ_c can be obtained by fitting a decay of transient photocurrent as a function of time (t) with a single-exponential function, $\exp(-t/\tau_c)$. The electron lifetime (τ_e) can also be obtained by fitting a decay of transient photovoltage with $\exp(-t/\tau_e)$. Figure 5(a) shows the electron diffusion coefficient (D_e) as a function of J_{sc} for NP and NR2 films. The D_e value of the NR2 film was slightly higher than that of the NP TiO_2 film. Figure 5(b) shows the electron life time (τ_e) as a function of J_{sc}. The τ_e values of the NR2 films turned out to be approximately twice, compared to those of the NP films. Larger D_e and τ_e suggests that TiO_2 nanorods are more efficient structure than the NP in regarding to the electron transport. This is caused by the intrinsic advantage

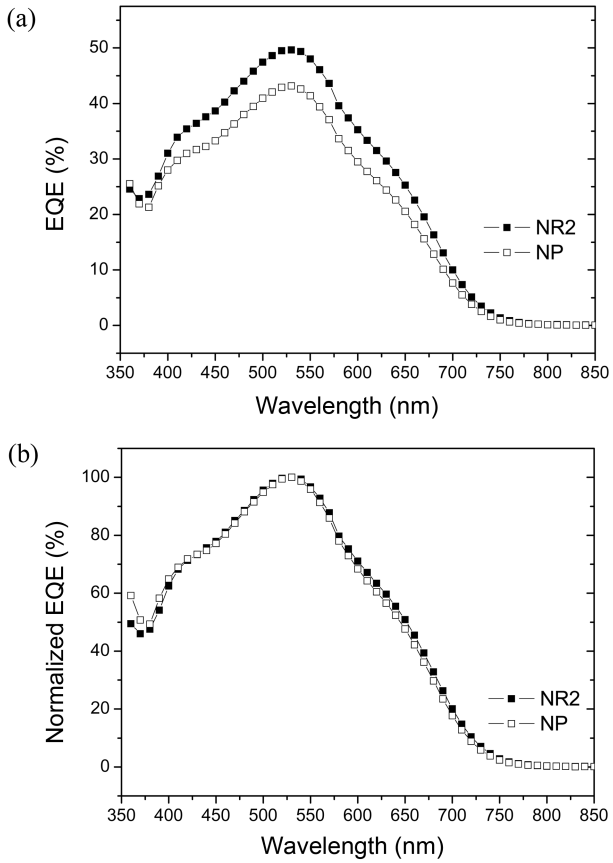

Figure 6. (a) IPCE spectra for the DSSCs derived from NP and NR2, and (b) their normalized spectra.

of TiO_2 nanorod structure, since the electron transport within the nanorod is highly efficient and the NR-based films will have relatively less grain boundaries than the NP-based films.

Diffusion lengths (L_e) in the several TiO_2 layers were also determined from diffusion coefficient and life time by the Eq. (2).[21,27]

$$L_e = (D_e \times \tau_e)^{1/2} \quad (2)$$

Figure 5(c) plots the J_{sc} *vs* L_e for the DSSC-NP and DSSC-NR2. The L_e values of NP and NR2 films were determined to be about 21.28 μm and 29.62 μm, respectively, suggesting that the photo-injected electrons in the NR2 can move considerably longer distance without recombination to the electrolyte.

The incident photon to current conversion efficiency (IPCE) spectra of the DSSC-NP and DSSC-NR2 are shown in Figure 6(a). In the entire wavelength region, DSSC-NR2 reveals higher external quantum efficiency (EQE) than DSSC-NP, which is compatible with the J_{sc} data obtained by I-V measurement. In order to estimate the light scattering effect, the IPCE spectra has been normalized, as shown in Figure 6(b). DSSC-NR2 showed slightly higher EQE in the long wavelength region around 600-750 nm, suggesting that the NR2 film provides an appreciable scattering effect. Generally, NR2 with a size of 4 × 15 nm does not show any significant scattering effect. It is considered that the observed scattering effect originates from the formation of the larger particles during the sintering at 500 °C.

Conclusions

The higher L_e and EQE of NR2 than that of NP suggests that NRs are more efficient structure for the electrons transport from dye molecules to FTO. As a result, the DSSC derived from the NR2 (4 × 15 nm) demonstrated significantly improved photovoltaic conversion efficiency compared to that of the NP (5 × 5.5 nm). That is, J_{sc} was significantly increased from 9.536 to 13.473 mA/cm^2, although V_{oc} was slightly decreased from 0.6643 to 0.6404 V. Hence, η was enhanced from 4.18% to 6.07%. Among the NRs, NR2 showed the highest η, because longer NRs than NR2 showed relatively higher resistance in the interface, due to the difficulty in tight contact and full coverage of the FTO substrate.

Acknowledgments. We gratefully acknowledge the financial support of the Korea Research Foundation (Grant No. D00007).

References

1. O'Regan, B.; Gratzel, M. *Nature* **1991**, 353, 737.
2. Jui, J.; Isoda, S.; Wang, F.; Adachi, M. *J. Phys. Chem. B* **2006**, *110*, 2087.
3. Adachi, M.; Murata, Y.; Takao, J.; Jiu, J.; Sakamoto, M.; Wang, F. *J. Am. Chem. Soc.* **2004**, *126*, 14943.
4. Papageogiou, N.; Barb, C.; Gratzel, M. *J. Phys. Chem. B* **1998**, *102*, 4156.
5. Gomez, M.; Lu, J.; Olsson, E.; Hagfeldt, A.; Granqvist, G. C. *Sol. Energy Mater. Sol. Cells* **2000**, *64*, 385.
6. Horiuchi, T.; Miura, H.; Uchida, S. *Chem. Commun.* **2003**, *24*, 3036.
7. Barzykin, A. V.; Tachiya, M. *J. Phys. Chem. B* **2004**, *108*, 8385.
8. Kay, A.; Gratzel, M. *Chem. Mater.* **2002**, *14*, 2930.
9. Song, M. Y.; Kim, D. K.; Ihn, K. J.; Jo, S. M.; Kim, D. Y. *Nanotechnology* **2004**, *15*, 1861.
10. Shankar, K.; Mor, G. K.; Prakasam, H. E.; Varghese, O. K.; Grimes, C. A. *Langmuir* **2007**, *23*, 12445.
11. Yoshida, K.; Jiu, J.; Naganatsu, D.; Nemoto, T.; Kurata, H.; Adachi, M.; Isoda, S. *Mol. Cryst. Liq. Cryst.* **2008**, *491*, 14.
12. Fujihara, K.; Kumar, A.; Jose, R.; Ramakrishna, S.; Uchida, S. *Nanotechnology* **2007**, *18*, 365709/1.
13. Lee, B. H.; Song, M. Y.; Jang, S. Y.; Jo, S. M.; Kwak, S. Y.; Kim, D. Y. *J. Phys. Chem. C* **2009**, *113*, 21453.
14. Wang, G. B.; Fu, M. G.; Li, B.; Du, G. P.; Li, L.; Qin, X. M.; Shi, Y. Z. *Appl. Phys. A* **2010**, *100*, 1169.
15. Yang, D. J.; Park, H.; Cho, S. J.; Kim, H. G.; Choi, W. Y. *J. Phys. Chem. Solids* **2008**, *69*, 1272.
16. Miao, L.; Tanemura, S.; Toh, S.; Kaneko, K.; Tanemura, M. J. *J. Cryst. Growth* **2004**, *264*, 246.
17. Cozzoli, P. D.; Kormowski, A.; Weller, H. *J. Am. Chem. Soc.* **2003**, *125*, 14539.
18. Saji, V. S.; Pyo, M. *Thin Solid Films* **2010**, *518*, 6542.
19. Baek, I. C.; Vithal, M.; Chang, J. A.; Yum, J. H.; Nazeeruddin, M. K.; Gratzel, M.; Chung, Y. C.; Seok, S. I. *Electrochem. Commun.* **2009**, *11*, 909.
20. Kim, E. Y.; Choi, H.; Whang, C. M. *J. Mater. Sci.* **2010**, *45*, 3895.
21. Nakade, S.; Kanzaki, T.; Wada, Y.; Yanagida, S. *Langmuir* **2005**,

21, 10803.
22. Lagemaat, J.; Park, N. G.; Frank, A. J. *J. Phys. Chem. B* **2000**, *104*, 2044.
23. Kern, R.; Sastrawan, R.; Ferver, J.; Stangl, R.; Luther, J. *Electrochim. Acta* **2002**, *47*, 4213.
24. Hoshikawa, T.; Yamada, M.; Kikuchi, R.; Eguchi, K. *J. Electrochem. Soc.* **2005**, *152*, E68.
25. Wang, Q.; Moster, J. E.; Gratzel, M. *J. Phys. Chem. B* **2005**, *109*, 14945.
26. Hauch, A.; Ceorg, A. *Electrochim. Acta* **2001**, *46*, 3457.
27. Bandic, Z. Z.; Bridger, P. M.; Piquette, E. C.; McGrill, T. C. *Appl. Phys. Lett.* **1998**, *73*, 3276.